A satellite blind spot masks crop residue burning across northern India

Ivar R. van der Velde*[1], Piyushkumar N. Patel[1], Ritesh Gautam[2], Guido R. van der Werf[3], Gareth Roberts[4] and Ilse Aben[1,5]

1. SRON Space Research Organisation Netherlands, Leiden, Netherlands
2. EDF Environmental Defense Fund, Washington DC, USA
3. Meteorology and Air Quality Group, Wageningen University and Research, Wageningen, Netherlands
4. School of Geography and Environmental Science, University of Southampton, Southampton, UK
5. Department of Earth Sciences, Vrije Universiteit, Amsterdam, Netherlands

*Corresponding author: I.R. van der Velde (I.R.van.der.Velde@sron.nl)

This is a non-peer reviewed preprint submitted to EarthArXiv

Abstract

Postmonsoon crop residue burning in the Indian states of Punjab and Haryana is a major source of air pollution and air quality degradation across the Indo-Gangetic Plain (IGP). Recent satellite observations have revealed an apparent inconsistency between declining fire detections and persistent or increasing atmospheric pollution. Here we combine eight years (2018-2025) of fire observations from low Earth orbiting (LEO) and geostationary satellites, satellite-derived atmospheric composition observations, ground-based air quality observations, meteorological reanalyses data, and chemical transport model simulations to investigate the drivers of this discrepancy. MODIS and VIIRS LEO observations indicate more than 90% decline in fire activity after 2021, whereas the geostationary SEVIRI observations reveal sustained or increasing fire activity. This divergence results primarily from fires started later in the day, beyond the time window the MODIS and VIIRS satellites pass over. Moreover, despite extensive burning, atmospheric pollution levels varied substantially between years. In Punjab, carbon monoxide and aerosol concentrations reached record levels in 2024 but were comparatively modest in 2025. Meteorological analyses indicate that persistent eastward winds in 2025 enhanced the transport of clean air into the IGP, substantially reducing atmospheric accumulation of pollutants. We conclude that changes in burn timing can substantially bias conventional fire monitoring systems and that meteorological variability and observational constraints imposed by cloud cover can be as important as emissions in interpreting regional air quality impacts.

Significance Statement

Crop residue burning contributes heavily to air pollution after the monsoon season across northern India. Satellite records from 2024-2025 reveal a puzzling contradiction: conventional fire detection instruments in low Earth orbit indicate declining fire activity, while atmospheric pollution observations show record high levels in 2024 and only modest levels in 2025. By combining geostationary, atmospheric composition, air quality, and meteorological data, we show agricultural burning has shifted towards late afternoon, outside the observation window of typical fire monitoring satellites. Year-to-year variations in atmospheric ventilation and cloud cover strongly affect pollution severity and detection capabilities. Accounting for these effects is important for improving fire emission inventories, air quality assessments, and air pollution mitigation across the Indo-Gangetic Plain.

Main Text

Introduction

Air pollution remains one of the most significant environmental and public health challenges in India. The Indo-Gangetic Plain (IGP), home to hundreds of millions of people, consistently ranks among the areas with the world's highest pollution levels[1,2,3]. During the postmonsoon months of October and November, widespread haze episodes frequently affect the IGP states of Punjab, Haryana, Delhi National Capital Region (Delhi-NCR), Uttar Pradesh, and adjacent areas[4]. These pollution events have been linked to respiratory and cardiovascular diseases[5,6], affecting growth of young adolescents[7], causing premature deaths[8], reducing visibility[9], and imposing substantial economic losses[10].

A major contributor to postmonsoon pollution is the burning of crop residues following rice harvest[11]. Mechanized harvesting leaves large quantities of straw and stubble on agricultural fields[12]. Farmers rely on burning as the most economical, quickest way to clear residues before the sowing of winter wheat[13,14]. The practice is particularly prevalent in Punjab and Haryana, where rice-wheat rotation dominates the local agricultural production[15].

The crop residue burning generates emissions that are a major source of fine particulate matter (PM2.5), contributing up to 50% of the PM2.5 concentrations in Punjab during peak burning periods[16], and significantly degrades air quality across the IGP[17,18]. Due to incomplete combustion processes, crop burning is also an important source of carbon monoxide (CO), and other trace gases[19]. Estimating emissions from biomass burning is difficult because fire detection and emission quantification are uncertain. Widely used inventories, such as the Global Fire Assimilation System[20] (GFAS) and the Global Fire Emission Database[21] (GFED), provide valuable estimates of fire-related emissions for this region, but their emissions can differ substantially. In addition to fires, other key sources of pollutants include transportation, industry, domestic fuel use and seasonal heating[22]. Therefore, the observed CO and PM2.5 concentrations over the region reflect multiple sources, including crop residue burning alongside other anthropogenic activities that influence regional air quality[19]. Typical meteorological conditions in late autumn and winter, such as weak winds, temperature inversions, low boundary layer heights, and high relative humidity, can further inhibit dispersion and contribute to the persistence and amplification of haze[23,24].

The contribution of fires to the total pollution remains uncertain because of limitations in existing fire monitoring systems[25,26], and due to uncertainties of the underlying assumptions of vegetation and combustion characteristics[27]. Most operational fire inventories rely on observations from sun-synchronous low Earth orbiting (LEO) satellites such as Terra and Aqua that carry the Moderate-resolution Imaging Spectroradiometer[28] (MODIS) and the Suomi-NPP, NOAA20 and NOAA21 satellites that carry the Visible Infrared Imaging Radiometer Suite[29] (VIIRS). These instruments are commonly used for fire activity and fire radiative power (FRP) monitoring but have a significant limitation in that each can observe at best a given location only twice a day (daytime and nighttime), and require near clear-sky conditions. During the day, the Terra and Aqua satellites had equatorial overpass times of approximately 10:30 and 13:30 local time (LT), respectively. Since 2022, however, both satellites have experienced orbital drift, with Terra's overpass time gradually shifting to about one hour earlier and Aqua's to about one hour later[30]. The three satellites carrying the VIIRS have an overpass time roughly between 13:30 and 13:45 LT at the equator. In regions like the IGP, where agricultural fires often burn for only 1-2 hours[15] and can occur at any time during the day, this limitation means many fires can go undetected. Additional constraints, including sensor spatial resolution, cloud cover and smoke further reduce the likelihood of detecting small scale agricultural fires[25].

An unexpected paradox emerged during the 2024 burning season. Satellite-derived fire detections fell to their lowest point since 2018, while atmospheric CO column concentrations from the TROPOspheric Monitoring Instrument[31] (TROPOMI) and aerosol optical depth (AOD) observations from Suomi-NPP/VIIRS[32,33] reached record highs. The contradiction raises questions about changing burning practices and the trustworthiness of satellite-based detection. Recent geostationary observations from both the Meteosat Second Generation-Indian Ocean Data Coverage (MSG-IODC) mission, carrying the Spinning Enhanced Visible and InfraRed Imager[34] (SEVIRI), and the Korean GEO-KOMPSAT-2A satellite, carrying the Advanced Meteorological Imager (AMI), suggest that the paradox arises because crop residue burning has shifted from early to late afternoon. As a result, more fires occur outside the overpass times of conventional LEO satellites and remain undetected. Singh et al.[35] documented a gradual shift in peak fire activity from approximately 13:30 LT in 2020 to around 17:00 LT in 2024 using SEVIRI retrievals, while Jethva[36] independently reported similar findings using GEO-KOMPSAT-2A AMI retrievals. While these studies established the shift toward late-afternoon burning using geostationary observations, its consequences for inferred fire emissions and regional pollution, and the extent to which meteorological variability affects the atmospheric response, remain poorly understood. Here, we combine fire observations with satellite and surface atmospheric composition measurements and chemical transport modeling to address these unknowns. Our analysis through 2025 will show an even more striking paradox: geostationary observations indicate even higher fire activity than in 2024, yet atmospheric pollution remains relatively low.

Here we address three key questions: (1) Have agricultural burning practices changed in recent years? (2) How do those changes affect satellite estimates of fire activity and emissions? (3) What is the role of meteorological variability on the severity of pollution across the IGP?

Results

Diverging trends in fire activity and atmospheric pollution

Figure 1 reveals diverging trends between satellite-detected fire activity and atmospheric pollution across northern India during the main part of the postmonsoon crop residue burning season (1-30 November). Fire detections and fire radiative power (FRP) declined sharply after 2021, while atmospheric pollution remained high, with 2024 standing out as an extreme example: CO and AOD reached the highest levels despite some of the lowest fire activity observed during the study period. By 2025, fire activity declined further, while CO and AOD remained only modestly elevated above pre-fire levels (1-10 October).

TROPOMI CO observations (Fig. 1a) show substantial year-to-year variability, with the highest concentrations in 2024 and the lowest in 2022 and 2025. VIIRS AOD (Fig. 1b) broadly follows these variations, but the relationship with CO is not strong. For example, AOD in 2023 was nearly as high as in 2024 despite substantially lower CO concentrations, pointing to additional sources and processes influencing aerosol loading across the IGP. These can include dust transport, secondary inorganic aerosol formation, construction and road dust, and episodic events such as Diwali festival[37-39], which increase the aerosol loading but with little contribution to atmospheric CO. It is noteworthy that Diwali occurred within the 1-30 November period in 2018, 2020, 2021, and 2023, on its boundary in 2024 (31 October - 1 November), but outside the analysis window in 2019, 2022, and 2025. Interestingly, the three years with the lowest AOD coincide with those in which Diwali fell outside the analysis period, suggesting that festival-related emissions may provide a modest secondary contribution to the observed AOD.

The pollution associated with the burning season extends well beyond the main source regions of Punjab and Haryana, with enhanced CO and aerosol loading spreading eastward across the IGP into densely populated regions including Delhi-NCR. Over Punjab, mean CO columns increased by approximately 20% during the burning season relative to the pre-fire period (Fig. 1d), while AOD increased by about 50% (Fig. 1e), consistent with previous studies linking crop residue burning to regional haze[40].

The sharp decline in observed fire activity is evident in the VIIRS record (Fig. 1c). In Punjab, seasonal FRP decreased by more than 90% relative to 2021 (Fig. 1f), even though substantial atmospheric pollution persisted in subsequent years. Haryana showed a similar, although less pronounced, decline. The mismatch is most pronounced in 2024, when record-high pollution coincided with very low satellite-detected fire activity. Conversely, the additional decline in FRP in 2025 was accompanied by only modest increases in CO and AOD above pre-fire levels. Together, these contrasting trends demonstrate that changes in satellite-detected fire activity cannot by themselves explain the observed variability in regional atmospheric pollution.

Diverging trends between LEO and geostationary sensors

To investigate why atmospheric pollution increased while LEO fire detections declined, we compared fire observations from LEO and geostationary satellites. Over Punjab and Haryana (Figs. 2a,c), MODIS and VIIRS show consistent interannual variability, including a decline in fire activity after 2021. Although both sensors exhibit similar variability, MODIS FRP is lower because its 1 km pixels detects fewer agricultural fires than VIIRS (375 m). MSG-IODC operates at a much coarser resolution over this region (>10 km), but nonetheless matches the temporal pattern in Punjab (2018-2022) and in Haryana (2018-2023). After that, the records diverge: while LEO observations continue to decline, MSG-IODC detects substantially higher FRP in 2024 and 2025. Restricting MSG-IODC observations to the MODIS/VIIRS overpass time window (13:00-14:30 LT) removes this discrepancy, with the geostationary record closely matching the declining LEO trends.

The close agreement between the time restricted MSG-IODC observations and the LEO record indicates that the divergence is driven primarily by temporal sampling rather than differences in sensor characteristics. It also suggests that an increasing fraction of agricultural burning now occurs outside the early-afternoon satellite overpass window. This shift is quantified by taking the ratio of MSG-IODC FRP detected outside versus inside the LEO overpass time window (Figs. 2b,d). In Punjab, outside-to-inside FRP ratios remained between 3 to 11 through 2022, it then increased sharply to 1000 by 2025, as the FRP within the overpass window declined below 0.1 GW, while seasonal total FRP peaked 800 GW. This suggests that a vast majority of detected burning occurred outside the LEO observation window. Haryana exhibits a similar trend, although burning outside the overpass period has been more common throughout the record. These results confirm recent work[35,36] showing a shift in peak crop residue burning from early to late afternoon, and our results demonstrate that it persisted through the 2025 burning season.

Shift in the diurnal cycle of biomass burning

The shift in burning behavior is particularly evident in the diurnal cycle of MSG-IODC FRP (Fig. 3a). During 2020-2021, a large fraction of the fire activity occurred in the early afternoon period sampled by MODIS and VIIRS. From 2023 onward, however, the diurnal distribution progressively moved to late afternoon, with peak burning occurring between 16:30 and 17:00 LT. The shift in burning reached its high point in 2025: late afternoon FRP was 2.5 times higher than in 2024, while the early afternoon FRP, during the MODIS/VIIRS overpass time window, remained extremely low and occasionally approached zero (Fig. 3b). The LEO sensors therefore missed most burning and underestimated fire activity.

Enhanced geostationary FRP in 2025 was distributed across much of southern Punjab (Fig. 3d), the main crop residue burning region, rather than being dominated by a few exceptionally large fires. The spatial pattern closely resembles what is observed in 2024 (Fig. 3c), suggesting that the increase reflects a systematic change in burning practices rather than a retrieval artefact. The anomaly was also mostly confined to Punjab. Across the full MSG-IODC domain, total November FRP continued to decline (SI Fig. S1), consistent with for example decreasing burned area in Africa associated with cropland expansion[41]. Viewed in this broader context, 2025 was a moderate fire year overall, indicating that the enhanced burning was a regional phenomenon rather than a continent wide increase.

Several factors may contribute to the shift toward later burning. Possible causes include governmental policies, benefits of drier fuels, limited daytime labor, and lower fire spread risk during calmer evenings[42]. Regardless of the cause, the implications for satellite fire monitoring are clear. Emission inventories that rely mainly on LEO observations are beginning to miss a large fraction of agricultural burning. GFED5, GFED4s, and GFAS all report declining emissions after 2021 (SI Fig.

S2), despite atmospheric observations and geostationary fire detections indicating sustained or increasing fire activity. These apparent emission reductions therefore reflect growing observational biases rather than actual decreases in agricultural fire emissions.

Independent evidence for the shift in burning

Ground-based air quality observations independently support the interpretation of the shift in burning. The Aakash monitoring network[16,43] recorded distinct PM2.5 pollution episodes during the 2022-2024 burning seasons, with the most severe event occurring in mid-November 2024 (SI Fig. S3a), consistent with the satellite-derived maxima in CO and AOD. In 2024, the mean diurnal cycle shows a pronounced late afternoon increase in PM2.5, between approximately 16:00 and 17:00 LT, coinciding with the MSG-IODC fire peak (SI Figs. S3b-e). By contrast, the morning decrease associated with boundary layer growth is nearly identical across all years, suggesting that enhanced afternoon pollution in 2024 is driven primarily by emissions rather than changes in atmospheric mixing. Surface CO measurements exhibit the same behavior (SI Fig. S4).

Visibility observations from the Amritsar station in Punjab (SI Fig. S5) provide further support. Fire season visibility in 2024 was exceptionally poor (<2 km during daytime), consistent with the record high CO and AOD observed from space, whereas visibility in 2025 was more moderate (2-3 km). The onset of the decline in daily visibility also shifted from about 13:00 LT in 2018 to approximately 15:00 LT in 2025, which lines up with the delayed timing of agricultural burning.

The MODIS MCD64A1 burned area product[44] provides an additional perspective (SI Fig. S6). Even though it shows a declining trend after 2022, burned area in Punjab increased by about 50% in 2025 compared to 2024. This is particularly notable, because MCD64A1 relies partially on MODIS active fire detections and is known to underestimate small, fragmented agricultural fires[45]. The observed shift towards late afternoon burning would further reduce the sensitivity to this kind of burning. Yet, the product still indicates more burned area in 2025, in agreement with the high fire activity detected by MSG-IODC.

Burned area estimates nevertheless remain highly uncertain in this region. MCD64A1, the VIIRS VNP64A1 product[46], and the Sentinel-3 Synergy (SYN) product[47] report similar overall burned area magnitudes but differ substantially in their interannual variability. VNP64A1 indicates a steady decline after 2022, whereas Sentinel-3 SYN (only available for 2019-2024 at time of writing) shows a pronounced increase in 2024. The discrepancy may come from the finer spatial resolution of Sentinel-3 (300 m versus 500 m for both MCD64A1 and VNP64A1), which improves the detection of small burns that are common across Punjab.

Influence of cloud cover on geostationary fire observations

Because satellite fire detections are strongly affected by cloud contamination, we examined the relationship between cloud cover from MODIS Multi-Angle Implementation of Atmospheric Correction (MAIAC) MCD19A2[48] and geostationary FRP over Punjab. The low cloud fractions during the 2025 burning season coincided with record-high MSG-IODC FRP, whereas the cloudiest year, 2019, recorded the lowest seasonal FRP (Fig. 4). Across the observational record, fire season FRP exhibits a strong inverse power-law relationship with cloud fraction, indicating that cloud cover has a significant effect on the assessment of fire activity from space. This relationship is also evident on daily timescales, with FRP peaking under clear conditions and declining sharply during cloudy periods (SI Fig. S7). Cloud cover and smoke contribute to both day-to-day and interannual variability in satellite-observed fire activity. The unusually clear conditions during 2025 therefore probably enhanced the exceptionally high FRP detected that year.

Cloud cover alone cannot explain the difference between LEO and geostationary observations. The late afternoon shift in burning remains evident regardless of cloud conditions. Instead, cloud cover primarily affects how much fire activity satellites can actually see, while the shift in burn timing affects whether fires are observed at all by early-afternoon LEO satellites.

Meteorological controls on pollution accumulation

Although fire activity was extensive during both 2024 and 2025, air pollution levels varied greatly. This contrast points to an important role for meteorological conditions in regulating pollutant accumulation. WRF-Chem simulations, nudged by NCEP FNL reanalysis, indicate that 2024 was characterized by weak and variable winds across the IGP and Punjab (Figs. 5a,b), whereas 2025 experienced persistently stronger eastward flow. Mean vector-averaged wind speeds in 2025 were approximately 2.5 times higher than in previous years, indicating efficient ventilation and increased horizontal transport.

A more detailed analysis of wind speed, wind direction, and TROPOMI CO is presented in SI Fig. S8. Strong eastward nighttime winds coincide with lower CO across the IGP, while daytime CO correlates primarily with wind speed. In Punjab, southward flow produces the lowest CO concentrations. HYSPLIT trajectory simulations support these findings. In 2024, air parcels remained largely over the IGP for nearly 10 days, indicating stagnant conditions (SI Fig. S9a). In contrast, 2025 trajectories originated over the Atlantic Ocean and passed through the IGP region rapidly, indicating efficient ventilation (SI Fig. S9b).

We used WRF-Chem to calculate a CO accumulation sensitivity metric (SI Fig. S10), which estimates the atmospheric CO increase per unit of fire emission. High sensitivities indicate pollutant accumulation over Punjab, whereas low sensitivities reflect efficient horizontal advection and dispersion. Modeled sensitivities correlate with observed CO enhancements with a Pearson correlation of $r=0.85$ ($p=0.008$, SI Fig. S11), highlighting the dominant influence of meteorological conditions on pollution severity. Years with comparable emissions can produce different air quality outcomes depending on prevailing atmospheric conditions.

An independent analysis supports this interpretation: for 2018-2023, the daytime ventilation coefficient derived from MERRA-2 reanalysis explains nearly all interannual variability in November AOD over Punjab ($r = -0.99$), suggesting the dominant role of vertical mixing in regulating aerosol accumulation during these years. In contrast, the AOD level in 2024 lies well above the ventilation coefficient relationship, consistent with exceptionally stagnant conditions combined with substantial fire emissions that were largely missed by LEO satellite observations. Conversely, the AOD level in 2025 falls below the relationship, indicating that horizontal advection by unusually persistent eastward winds outweighed the influence of reduced vertical mixing, leading to lower AOD than would be expected from the ventilation coefficient alone (SI Fig. S12b).

Discussion

Recent changes in the dynamics of crop residue burning across northern India cannot be understood from conventional satellite fire detections alone. Building on new studies that used geostationary sensors, we show that agricultural burning has progressively shifted toward late afternoon, outside the overpass window of commonly used LEO satellites such as MODIS and VIIRS[35,36]. This observational bias affects fire inventories, leading to persistent underestimation of emissions, and can provide misleading interpretations of fire activity and its contribution to regional air pollution. By 2025, LEO fire detections had declined by more than 90% relative to 2021, whereas geostationary observations indicated burning remained high.

The implications extend well beyond northern India. LEO satellites sample at best any given location only a few times each day, making them inherently sensitive to changes in the timing of short-lived fires. Agricultural burning, which often occurs within narrow daytime windows, is particularly vulnerable to this sampling bias. Consequently, apparent long-term trends in satellite-derived fire activity may partly reflect changing burning timings rather than genuine changes in emissions. Fire products and emission inventories that rely primarily on LEO observations should therefore be interpreted with caution unless their trends are supported by secondary observations.

The striking contrast between 2024 and 2025 highlights that fire activity alone cannot explain the severity of postmonsoon pollution episodes. Year-to-year differences in air pollution reflect not only emissions from fire activity, but also meteorological transport and ventilation. Although burning activity appeared higher in 2025 (possibly due to clear-sky conditions) than in 2024, stronger eastward winds provided rapid transport and ventilation throughout the IGP, preventing the extreme accumulation of pollutants observed during the stagnant conditions of 2024. Aerosol-radiation feedbacks may have further enhanced pollution in 2024 by increasing lower tropospheric stability and suppressing vertical mixing[40].

Satellite observations of fires and atmospheric composition are all affected by observing conditions, although in different ways. Fire detections from both LEO and geostationary sensors are restricted under cloudy conditions, meaning the exceptionally clear 2025 season likely increased the number of detected fires independent of any real change in burning activity. Atmospheric composition retrievals are also influenced by clouds: AOD retrievals generally require cloud-free scenes, whereas TROPOMI CO retrievals can often be obtained in the presence of low-level clouds but not under high-level cloud cover. In addition, dense smoke can be misclassified as cloud or assigned lower retrieval quality, removing the most polluted scenes from the record. Consequently, interannual differences in satellite-derived fire emissions, CO, and aerosol loading reflect a combination of real variability in fire activity and limitations in observing conditions. The high CO and aerosol levels observed in 2024 are therefore, if anything, likely underestimated, implying that the true contrast with 2025 may be even larger than reported. Surface PM2.5, CO, and visibility observations, which are unaffected by these satellite screening effects, independently confirm the pronounced interannual differences as shown in this study.

Interpreting postmonsoon air pollution therefore requires consideration of three interacting processes: 1) a shift in agricultural burning practices that impact satellite detectability, 2) observational limitations associated with satellite sampling and cloud cover, and 3) meteorological conditions that can impact pollutant accumulation and transport. Geostationary fire observations are often overlooked but complement LEO sensors because they can potentially see the complete diurnal cycle of burning and therefore reveal changes in agricultural burning practices that would otherwise remain undetected.

These results are also important for public health and air quality management. Previous work estimated that burning a few hours earlier than 14:30 LT reduced regional pollution exposure by about 14% and could prevent roughly 10,000 premature deaths per year. Delaying burning into the late afternoon increased health impacts by up to 30%[49]. This sensitivity exists because the planetary boundary layer reaches its maximum depth during early afternoon before rapidly collapsing later in the day, reducing vertical mixing and promoting accumulation of smoke near the surface. Consistent with this mechanism, MERRA-2 reanalysis shows that the November boundary layer over Punjab at the current fire peak (16:30–17:30 LT) is typically less than half as deep as during the MODIS/VIIRS overpass window, and in 2025 reached only about one-fifth of that depth (≈300 m, SI Fig. S12a). The observed shift in burn timing therefore injects smoke into a several-fold shallower mixing layer, amplifying near-surface exposure. It highlights that even low-cost interventions focused on burn timing could be meaningful in reducing the health burden of crop residue burning, and as shown in this work, such changes can be tracked from space.

The reasons why burning happens later remain uncertain. Factors such as labor availability, fuel moisture, and fire control considerations may contribute[42]. A recent survey[15] indicates that most burning occurs during daylight, with over half taking place between 14:00 and 18:00 LT. However, another possibility is that farmers are trying to remain hidden from satellite-based monitoring on purpose to avoid regulatory enforcement[35]. Because many reporting systems rely on MODIS and VIIRS detections, moving burning outside the typical satellite overpass time windows greatly lowers detection chances, a phenomenon that has also been reported for agricultural burning in China[50]. Although our observations cannot establish intent, the near-complete shift of burning outside the LEO observation window is consistent with this possibility. If such a change is occurring, it underscores the need for monitoring and regulatory frameworks that integrate geostationary fire observations with atmospheric composition measurements and ground-based monitoring networks. Such a holistic observing system would be more resilient to evolving burning practices while at the same time improving fire emission estimates, air quality forecasting, and mitigation policies.

Materials and methods

A concise description of the datasets, modeling framework, and analysis methods is provided below. More detailed descriptions of satellite retrieval algorithms, data processing, model configuration, parameterizations, emission inventories, and sensitivity analyses are provided in the SI.

1. Satellite observations

Total column carbon monoxide (CO) retrievals were obtained from the TROPOspheric Monitoring Instrument (TROPOMI) aboard Sentinel-5 Precursor satellite in the shortwave infrared band (2305-2385 nm) using the SICOR algorithm[31,51]. We retained retrievals with quality assurance values ≥0.7, corresponding to recommended clear-sky and low-cloud conditions.

Aerosol optical depth (AOD) was obtained from the Visible Infrared Imaging Radiometer Suite (VIIRS) aboard Suomi-NPP using the Deep Blue 550-nm product[33]. Fire Radiative Power (FRP) came from the MODIS Collection 6 active fire products[28] (Terra and Aqua) and VIIRS active fire products[29] (Suomi-NPP, NOAA-20, and NOAA-21). MODIS provides FRP at 1 km resolution, whereas VIIRS provides improved 375-m resolution and greater sensitivity to smaller fires.

Burned area was quantified using the MODIS MCD64A1[44], VIIRS VNP64A1[46], and Sentinel-3 SYN[47] burned area products. These datasets provide burned areas, using reflectance and thermal features, at spatial resolutions ranging from 300 m (Sentinel-3 SYN) to 500 m (MODIS and VIIRS).

To characterize the full diurnal cycle of fire activity, FRP retrievals came from the Spinning Enhanced Visible and InfraRed Imager (SEVIRI) aboard Meteosat-8/9 operating in the Indian Ocean Data Coverage configuration[34]. SEVIRI provides observations every 15 min, enabling detection of short-lived fire activity that is often missed by LEO satellites despite its coarser (>10 km) spatial resolution. Daily cloud fraction was obtained from the MODIS MAIAC MCD19A2 product[48].

2. Surface observations

We used surface air quality measurements from the Aakash Project Compact and Useful PM2.5 Instrument with Gas sensors (CUPI-G) network deployed across

Punjab, Haryana, and the Delhi National Capital Region during post-monsoon campaigns between 2022 and 2024[16,43]. Approximately 30-32 instruments continuously measured PM2.5 and CO, providing high frequency observations across both source and downwind regions. The Amritsar meteorological station provided surface visibility observations (data accessed via NOAA Climate Data Online) as an independent measure of aerosol loading.

3. Atmospheric modeling

Meteorological and chemical processes were simulated using Weather Research and Forecasting model coupled with chemistry (WRF-Chem) version 4.7.1[52] over northern India for September-December during 2018-2025 with 30 km horizontal resolution. We used the Regional Acid Deposition Model, second generation for gas-phase chemistry[53] (RADM2) for CO chemistry, while meteorological forcing was provided by the National Centers for Environmental Prediction (NCEP) Final (FNL) Operational Global Analysis dataset[54] to maintain consistency with observed meteorological conditions. In the model 33 vertical levels are defined with enhanced resolution in the boundary layer. The physical parameterizations[55-59] used are listed in the SI. Simulated CO profiles were convolved with TROPOMI averaging kernels before comparing to satellite observations.

Initial and lateral chemical boundary conditions came from the Copernicus Atmosphere Monitoring Service (CAMS) atmospheric composition reanalysis product[60]. For biomass burning emissions we used daily GFED5 emissions[61] through 2022 and the near-real-time GFED5-NRT product[62] thereafter. Anthropogenic and biogenic emissions were taken from the CAMS-GLOB-ANT v5.1[63] and CAMS-GLOB-BIO v3.0[64] inventories, respectively, and regridded to the model domain.

Air-mass transport was examined using HYSPLIT back-trajectory analyses[65], further discussed in the SI.

Planetary boundary layer (PBL) and wind diagnostics were additionally derived from the Modern-Era Retrospective Analysis for Research and Applications, Version 2 (MERRA-2) reanalysis[67]: hourly 10 m winds (M2T1NXSLV) and planetary boundary layer height (M2T1NXFLX) for October-November 2018-2025 over northern India. The ventilation coefficient was computed as the product of boundary layer height and 10 m wind speed.

4. Biomass burning accumulation sensitivity experiments

To quantify the influence of crop residue burning on regional CO accumulation over Punjab, we ran two WRF-Chem simulations per year: a baseline with all emissions everywhere and a sensitivity run that excluded biomass-burning emissions in five IGP states (Punjab, Haryana, Uttar Pradesh, Bihar, West Bengal). The contribution of biomass burning was calculated from the difference between the baseline and sensitivity simulations. To isolate the efficiency of atmospheric accumulation, the simulated CO enhancement over Punjab was divided by the corresponding fire emissions from Punjab.

Acknowledgments

This research was supported by funding from ESA Living Planet Fellowship program (No. 4000140029/22/I-DT-lr) and the NSO TROPOMI National Program. The WRF-Chem model computations were carried out on the National Supercomputer Snellius supported by SURF (https://www.surf.nl).

References

1. N. Ojha et al., On the widespread enhancement in fine particulate matter across the Indo-Gangetic Plain towards winter. Sci. Rep. 10, 5862 (2020).
2. V. Singh, S. Singh, N. Sharma, et al., Estimation of surface PM2.5 over the Indo-Gangetic Basin using MERRA-2 reanalysis and machine learning. Sci. Rep. 16, 13755 (2026).
3. J. P. Terry, G. Jia, R. Boldi, S. Khan, The Delhi "gas chamber": Smog, air pollution and the health emergency of November 2017. Weather 73, 348–352 (2018).
4. T. Kotrike, V. Sridhar, Tracing the haze: Satellite-based assessment of stubble burning and air quality in Delhi. Air Qual. Atmos. Health 19, 1 (2026).
5. K. Balakrishnan, S. Dey, T. Gupta, et al., The impact of air pollution on deaths, disease burden, and life expectancy across the states of India: The Global Burden of Disease Study 2017. Lancet Planet. Health 3, e26–e39 (2019).
6. S. Jain, S. K. Sharma, N. Vijayan, T. K. Mandal, Seasonal characteristics of aerosols (PM2.5 and PM10) and their source apportionment using PMF: A four-year study over Delhi, India. Environ. Pollut. 262, 114337 (2020).
7. P. Singh, S. Dey, Crop burning and forest fires: Long-term effect on adolescent height in India. Resour. Energy Econ. 65, 101240 (2021).
8. S. D. Ghude, D. M. Chate, C. Jena, G. Beig, R. Kumar, M. C. Barth, G. G. Pfister, S. Fadnavis, P. Pithani, Premature mortality in India due to PM2.5 and ozone exposure. Geophys. Res. Lett. 43, 4650–4658 (2016).
9. J. Rathore, D. Ganguly, V. Singh, M. Gupta, V. J. Vazhathara, A. Biswal, et al., Characteristics of haze pollution events during biomass burning period at an upwind site of Delhi. J. Geophys. Res. Atmos. 130, e2024JD042347 (2025).
10. A. Pandey, M. Brauer, M. Cropper, et al., Health and economic impact of air pollution in the states of India: The Global Burden of Disease Study 2019. Lancet Planet. Health 5, e25–e38 (2021).
11. K. V. S. Badarinath, T. R. Kiran Chand, V. Krishna Prasad, Agriculture crop residue burning in the Indo-Gangetic plains—A study using IRS-P6 AwiFS satellite data. Curr. Sci. 91, 1085–1089 (2006).

12. P. Kumar, S. Kumar, L. Joshi, eds., *Socioeconomic and Environmental Implications of Agricultural Residue Burning: A Case Study of Punjab, India* (Springer, New Delhi, 2015).

13. T. Liu, L. J. Mickley, R. Gautam, M. K. Singh, R. S. DeFries, M. E. Marlier, Detection of delay in post-monsoon agricultural burning across Punjab, India: Potential drivers and consequences for air quality. Environ. Res. Lett. 16, 014012 (2021).

14. D. B. Lobell, J. I. Ortiz-Monasterio, A. M. Sibley, V. S. Sohu, Satellite detection of earlier wheat sowing in India and implications for yield trends. Agric. Syst. 115, 137–143 (2013).

15. T. Liu, L. J. Mickley, S. Singh, M. Jain, R. S. DeFries, M. E. Marlier, Crop residue burning practices across north India inferred from household survey data: Bridging gaps in satellite observations. Atmos. Environ. X 8, 100091 (2020).

16. P. K. Patra, N. Yasutomi, H. Araki, A. Biswal, et al., *Aakash Project: Towards Mitigating Particulate Air Pollution for Improved Public Health Along with Sustainable Agriculture in Northwest India. Summary of Research Outcomes for Stakeholders During 2020–2025* (2025), pp. 1–52.

17. P. Khatri, T. Hayasaka, P. K. Patra, et al., Unveiling the effects of post-monsoon agricultural biomass burning on aerosols, clouds, and radiation in Northwest India. Prog. Earth Planet. Sci. 12, 11 (2025).

18. H. Jethva, O. Torres, R. D. Field, et al., Connecting crop productivity, residue fires, and air quality over northern India. Sci. Rep. 9, 16594 (2019).

19. I. N. Dekker, S. Houweling, S. Pandey, M. Krol, T. Röckmann, T. Borsdorff, J. Landgraf, I. Aben, What caused the extreme CO concentrations during the 2017 high-pollution episode in India? Atmos. Chem. Phys. 19, 3433–3445 (2019).

20. J. W. Kaiser et al., Biomass burning emissions estimated with a global fire assimilation system based on observed fire radiative power. Biogeosciences 9, 527–554 (2012).

21. G. R. van der Werf, J. T. Randerson, L. Giglio, T. T. van Leeuwen, Y. Chen, B. M. Rogers, M. Mu, M. J. E. van Marle, D. C. Morton, G. J. Collatz, R. J. Yokelson, P. S. Kasibhatla, Global fire emissions estimates during 1997–2016. Earth Syst. Sci. Data 9, 697–720 (2017).

22. S. K. Guttikunda, G. Calori, A GIS-based emissions inventory at 1 km × 1 km spatial resolution for air pollution analysis in Delhi, India. Atmos. Environ. 67, 101–111 (2013).

23. S. Choudhury, H. Rajpal, A. K. Saraf, S. Panda, Mapping and forecasting of North Indian winter fog: An application of spatial technologies. Int. J. Remote Sens. 28, 3649–3663 (2007).

24. T. Liu, M. E. Marlier, R. S. DeFries, D. M. Westervelt, K. R. Xia, A. M. Fiore, L. J. Mickley, D. H. Cusworth, G. Milly, Seasonal impact of regional outdoor biomass burning on air pollution in three Indian cities: Delhi, Bengaluru, and Pune. Atmos. Environ. 172, 83–92 (2018).

25. D. H. Cusworth, L. J. Mickley, M. P. Sulprizio, T. Liu, M. E. Marlier, R. S. DeFries, S. K. Guttikunda, P. Gupta, Quantifying the influence of agricultural fires in northwest India on urban air pollution in Delhi, India. Environ. Res. Lett. 13, 044018 (2018).

26. M. Kajino, K. Ishijima, J. Ching, K. Yamaji, R. Ishikawa, T. Kajikawa, T. Singh, T. Nakayama, Y. Matsumi, K. Kojima, T. Machida, T. Maki, P. K. Patra, S. Hayashida, Impact of post-monsoon crop residue burning on PM2.5 over northern India: Optimizing emissions using a high-density in situ surface observation network. Atmos. Chem. Phys. 25, 7137–7160 (2025).

27. G. R. van der Werf, J. T. Randerson, L. Giglio, G. J. Collatz, M. Mu, P. S. Kasibhatla, D. C. Morton, R. S. DeFries, Y. Jin, T. T. van Leeuwen, Global fire emissions and the contribution of deforestation, savanna, forest, agricultural, and peat fires (1997–2009). Atmos. Chem. Phys. 10, 11707–11735 (2010).

28. L. Giglio, J. Descloitres, C. O. Justice, Y. J. Kaufman, An enhanced contextual fire detection algorithm for MODIS. Remote Sens. Environ. 87, 273–282 (2003).

29. W. Schroeder, P. Oliva, L. Giglio, I. Csiszar, The new VIIRS 375 m active fire detection data product: Algorithm description and initial assessment. Remote Sens. Environ. 143, 85–96 (2014).

30. National Aeronautics and Space Administration, *NASA Applied Sciences: FireSense Executive Summary*. Available at https://nspires.nasaprs.com/external/viewrepositorydocument/cmdocum

entid=929460/solicitationId=%7B19F4296E-5280-3996-3149-42CB166328DC%7D/viewSolicitationDocument=1. Accessed 22 July 2026.

31. J. P. Veefkind et al., TROPOMI on the ESA Sentinel-5 Precursor: A GMES mission for global observations of the atmospheric composition for climate, air quality and ozone layer applications. Remote Sens. Environ. 120, 70–83 (2012).
32. A. Lyapustin, *VIIRS/NPP Land Aerosol Optical Depth Daily L2G Global 750 m RSIN Grid V002* (NASA Land Processes Distributed Active Archive Center, 2025).
33. Hsu, C., J. and Lee, V. Kim, Continuity Atmosphere L2 VIIRS Aerosol Deep Blue (AERDB_L2_VIIRS_SNPP), SIPS Processing System, University of Wisconsin (2019).
34. M. J. Wooster, G. Roberts, P. H. Freeborn, W. Xu, Y. Govaerts, R. Beeby, J. He, A. Lattanzio, R. Mullen, Meteosat SEVIRI Fire Radiative Power (FRP) products from the Land Surface Analysis Satellite Applications Facility (LSA SAF)—Part 1: Algorithms, product contents and analysis. Atmos. Chem. Phys. 15, 13217–13239 (2015).
35. N. Singh, R. Pradhan, B. P. Shukla, M. R. Pandya, Evidence of shift in stubble burning timing over northwest India from geostationary satellite observations. Curr. Sci. 129, 921–923 (2025).
36. H. Jethva, Timing the flames: Geostationary satellite detection of diurnally shifting stubble burning in northwestern India. Remote Sens. 18, 1506 (2026).
37. A. Singh, N. Rastogi, A. Patel, D. Singh, Seasonality in size-segregated ionic composition of ambient particulate pollutants over the Indo-Gangetic Plain: Source apportionment using PMF. Environ. Pollut. 219, 906–915 (2016).
38. C. Manchanda et al., Chemical speciation and source apportionment of ambient PM2.5 in New Delhi before, during, and after the Diwali fireworks. Atmos. Pollut. Res. 13, 101428 (2022).
39. U. C. Dumka, S. N. Tripathi, A. Misra, D. M. Giles, T. F. Eck, R. Sagar, B. N. Holben, Latitudinal variation of aerosol properties from the Indo-Gangetic Plain to central Himalayan foothills during the TIGERZ campaign. J. Geophys. Res. Atmos. 119, 4750–4769 (2014).

40. R. Gautam, P. N. Patel, M. K. Singh, T. Liu, L. J. Mickley, H. Jethva, R. S. DeFries, Extreme smog challenge of India intensified by increasing lower tropospheric stability. Geophys. Res. Lett. 50, e2023GL103105 (2023).

41. N. Andela, G. R. van der Werf, Recent trends in African fires driven by cropland expansion and El Niño to La Niña transition. Nat. Clim. Change 4, 791–795 (2014).

42. J. Erbaugh, G. Singh, Z. Luo, G. Koppa, J. Evans, P. Shyamsundar, Farmer perspectives on crop residue burning and sociotechnical transition in Punjab, India. J. Rural Stud. 111, 103387 (2024).

43. T. Singh, Y. Matsumi, T. Nakayama, et al., Very high particulate pollution over northwest India captured by a high-density in situ sensor network. Sci. Rep. 13, 13201 (2023).

44. L. Giglio, L. Boschetti, D. P. Roy, M. L. Humber, C. O. Justice, The Collection 6 MODIS burned area mapping algorithm and product. Remote Sens. Environ. 217, 72–85 (2018).

45. J. V. Hall, F. Argueta, M. Zubkova, Y. Chen, J. T. Randerson, L. Giglio, GloCAB: Global cropland burned area from mid-2002 to 2020. Earth Syst. Sci. Data 16, 867–885 (2024).

46. L. Giglio, L. Boschetti, D. P. Roy, J. V. Hall, M. Zubkova, M. Humber, H. Huang, V. Oles, The NASA VIIRS burned area product, global validation, and intercomparison with the NASA MODIS burned area product. Remote Sens. Environ.331, 114276 (2025).

47. J. Lizundia-Loiola, M. Franquesa, A. Khairoun, E. Chuvieco, Global burned area mapping from Sentinel-3 Synergy and VIIRS active fires. Remote Sens. Environ. 282, 113298 (2022).

48. A. Lyapustin, Y. Wang, *MODIS Multi-Angle Implementation of Atmospheric Correction (MAIAC) Data User's Guide, Collection 6.1, Version 3.1* (NASA Land Processes Distributed Active Archive Center, 2022).

49. R. Lan, S. D. Eastham, T. Liu, et al., Air quality impacts of crop residue burning in India and mitigation alternatives. Nat. Commun. 13, 6537 (2022).

50. Q. Lv, Z. Yang, Z. Chen, M. Li, B. Gao, J. Yang, X. Chen, B. Xu, Crop residue burning in China (2019–2021): Spatiotemporal patterns, environmental

impact, and emission dynamics. Environ. Sci. Ecotechnol. 21, 100463 (2024).

51. J. Landgraf, J. aan de Brugh, R. Scheepmaker, T. Borsdorff, H. Hu, S. Houweling, A. Butz, I. Aben, O. Hasekamp, Carbon monoxide total column retrievals from TROPOMI short-wave infrared measurements. Atmos. Meas. Tech. 9, 4955–4975 (2016).
52. G. A. Grell, S. E. Peckham, R. Schmitz, S. A. McKeen, G. Frost, W. C. Skamarock, B. Eder, Fully coupled "online" chemistry within the WRF model. Atmos. Environ. 39, 6957–6975 (2005).
53. W. R. Stockwell, P. Middleton, J. S. Chang, X. Tang, The second-generation regional acid deposition model chemical mechanism for regional air quality modeling. J. Geophys. Res. 95, 16343–16367 (1990).
54. National Centers for Environmental Prediction, *NCEP FNL Operational Model Global Tropospheric Analyses, Continuing from July 1999*. Research Data Archive, National Center for Atmospheric Research, Computational and Information Systems Laboratory (2000).
55. H. Morrison, J. A. Curry, V. I. Khvorostyanov, A new double-moment microphysics parameterization for application in cloud and climate models. Part I: Description. J. Atmos. Sci. 62, 1665–1677 (2005).
56. M. J. Iacono, J. S. Delamere, E. J. Mlawer, M. W. Shephard, S. A. Clough, W. D. Collins, Radiative forcing by long-lived greenhouse gases: Calculations with the AER radiative transfer models. J. Geophys. Res. Atmos. 113, D13103 (2008).
57. M. B. Ek, K. E. Mitchell, Y. Lin, E. Rogers, P. Grunmann, V. Koren, G. Gayno, J. D. Tarpley, Implementation of Noah land surface model advances in the National Centers for Environmental Prediction operational mesoscale Eta model. J. Geophys. Res. Atmos. 108, D22 (2003).
58. G. Grell, J. Dudhia, D. A. Stauffer, *A Description of the Fifth-Generation Penn State/NCAR Mesoscale Model (MM5)*(NCAR Tech. Note NCAR/TN-398+STR, National Center for Atmospheric Research, Boulder, CO, 1994).
59. S.-Y. Hong, Y. Noh, J. Dudhia, A new vertical diffusion package with an explicit treatment of entrainment processes. Mon. Weather Rev. 134, 2318–2341 (2006).

60. A. Inness, M. Ades, A. Agustí-Panareda, J. Barré, A. Benedictow, A.-M. Blechschmidt, et al., The CAMS reanalysis of atmospheric composition. Atmos. Chem. Phys. 19, 3515–3556 (2019).

61. G. R. van der Werf, J. T. Randerson, D. van Wees, et al., Landscape fire emissions from the fifth version of the Global Fire Emissions Database (GFED5). Sci. Data 12, 1870 (2025).

62. Y. Chen, G. R. van der Werf, M. Mu, D. van Wees, J. V. Hall, L. Giglio, R. Vernooij, D. C. Morton, L. Xu, T. Liu, R. C. Scholten, S. R. Coffield, M. B. Follette-Cook, L. Ott, J. T. Randerson, Tracking recent extremes and interannual variability of global fire emissions using a near-real-time extension to the Global Fire Emissions Database. Earth Syst. Sci. Data Discuss. (2026), in review.

63. A. Soulié, C. Granier, S. Darras, N. Zilbermann, T. Doumbia, M. Guevara, J.-P. Jalkanen, S. Keita, C. Liousse, M. Crippa, D. Guizzardi, R. Hoesly, S. J. Smith, Global anthropogenic emissions (CAMS-GLOB-ANT) for the Copernicus Atmosphere Monitoring Service simulations of air quality forecasts and reanalyses. Earth Syst. Sci. Data 16, 2261–2279 (2024).

64. C. Granier, S. Darras, H. Denier van der Gon, J. Doubalova, N. Elguindi, B. Galle, et al., *The Copernicus Atmosphere Monitoring Service Global and Regional Emissions* (Copernicus Atmosphere Monitoring Service, 2019).

65. A. F. Stein, R. R. Draxler, G. D. Rolph, B. J. B. Stunder, M. D. Cohen, F. Ngan, NOAA's HYSPLIT atmospheric transport and dispersion modeling system. Bull. Am. Meteorol. Soc. 96, 2059–2077 (2015).

66. M. K. Sha, B. Langerock, J.-F. L. Blavier, et al., Validation of methane and carbon monoxide from Sentinel-5 Precursor using TCCON and NDACC-IRWG stations. Atmos. Meas. Tech. 14, 6249–6304 (2021).

67. R. Gelaro, R., W. McCarty, M. J., Suárez, A. M. da Silva, R., Todling, A., Molod, A., et al, The Modern-Era Retrospective Analysis for Research and Applications, Version 2 (MERRA-2). Journal of Climate, 30(14), 5419–5454 (2017).

Main text figures

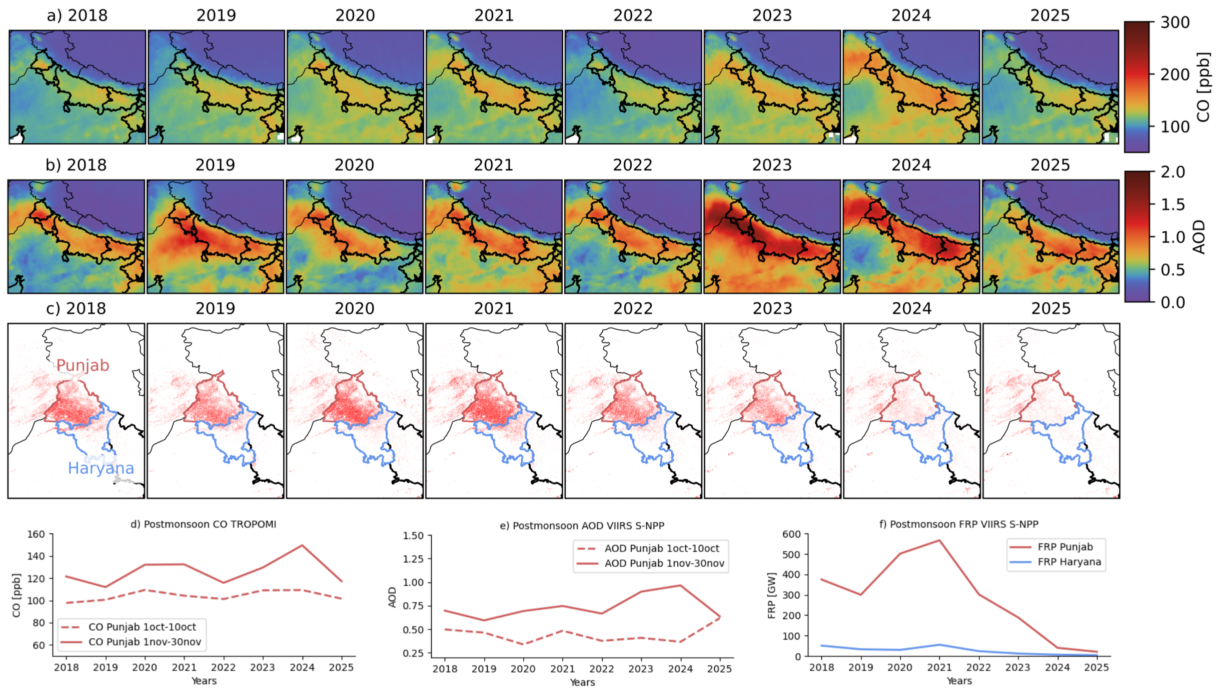

Figure 1. Panels (a) and (b) show maps of TROPOMI CO mole fraction [ppb] and VIIRS S-NPP AOD, respectively, over Northern India during the postmonsoon fire season (1-30 Nov). It shows strong interannual variability in pollution with record-high CO and AOD in 2024 and lows in 2019, 2022 and 2025. Outline of IGP is highlighted by the bold border line, showing from west to east the states of Punjab, Haryana, Delhi-NCR, Uttar Pradesh, Bihar, and West Bengal. Panel (c) displays the daily VIIRS S-NPP active fire detections zoomed in on Punjab (red) and Haryana (blue), revealing a declining trend in fire detections since 2022. Panels (d) and (e) present seasonal averages of CO and AOD during the fire season (1-30 Nov; solid red line) and before the fire season (1-10 Oct; dashed red line) for Punjab. It illustrates enhanced levels of pollution in November relative to the weeks prior as a result of crop residue burning. Panel (f) shows the total VIIRS S-NPP FRP for Punjab and Haryana, highlighting the aforementioned drop in fire activity since 2022, and the large difference in fire activity between the two neighboring states.

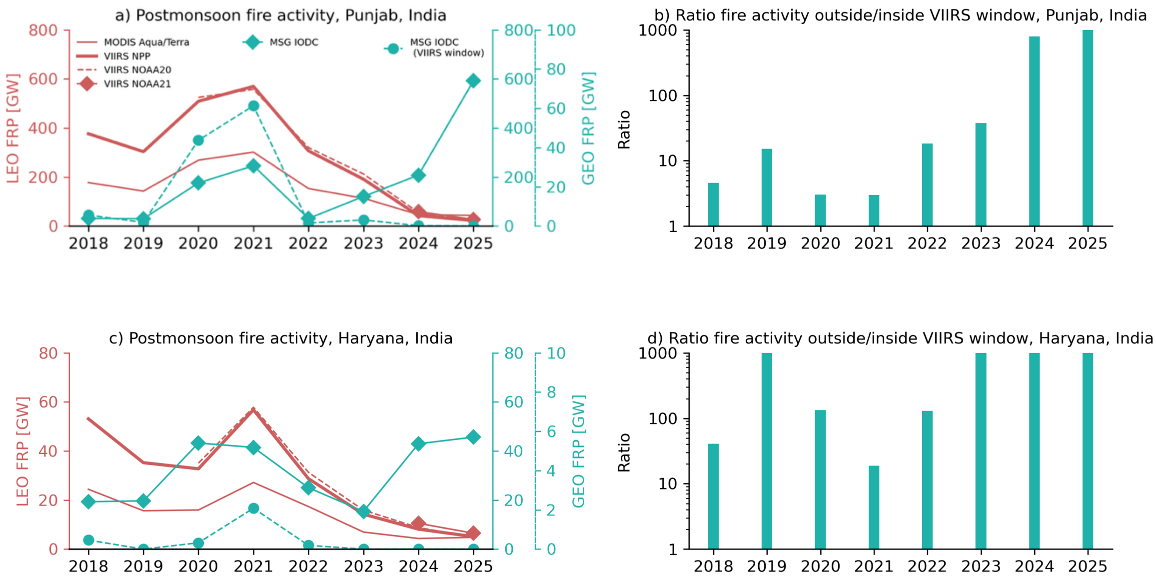

Figure 2. Panel (a) shows an 8-year time series of FRP [GW] for Punjab derived from LEO instruments MODIS and VIIRS (red) and geostationary MSG-IODC (solid green and solid green axis). While LEO instruments exhibit among them a consistent interannual variability, including a sharp decline since 2022, MSG-IODC detects a sharp increase from 2023 onward. Filtering MSG-IODC to the MODIS/VIIRS overpass time window (green dashed line and dashed axis) aligns its variability with MODIS/VIIRS, indicating temporal sampling differences as the primary cause of discrepancy. Panel (b) shows the ratio of MSG-IODC FRP detected outside versus inside the MODIS/VIIRS overpass time window (13:00-14:30 LT), showing that much burning in Punjab occurs outside the early afternoon overpass period. This fraction has risen since 2022, reaching nearly 1000:1. Panels (c-d) show the same results for Haryana. Similar to Punjab, MSG-IODC shows an increase in fire activity in 2024 and 2025, in contrast to MODIS and VIIRS detections. Fire activity has also been persistently higher outside the VIIRS overpass time window, and to a greater extent than in Punjab.

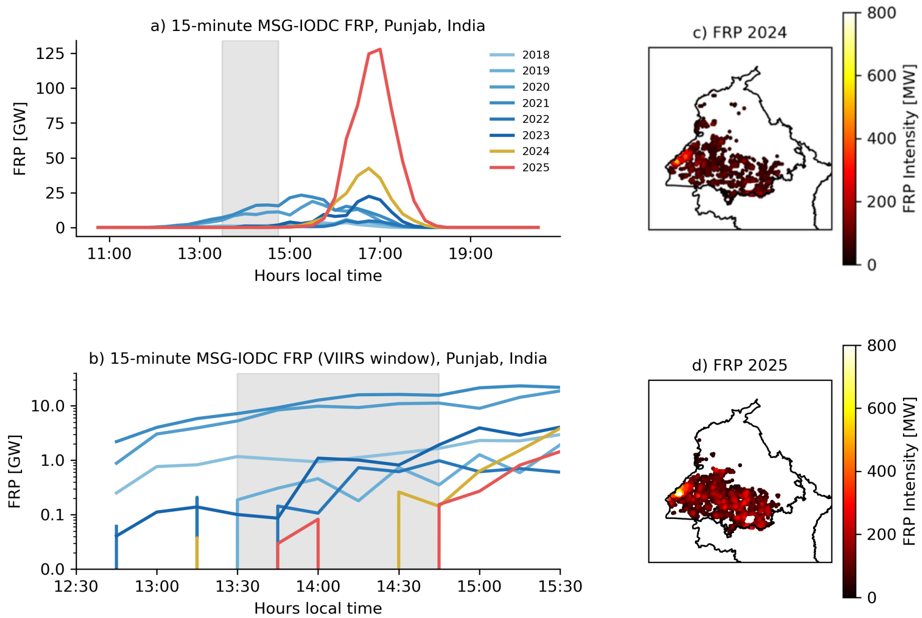

Figure 3. Panel (a) shows the diurnal cycle of MSG-IODC FRP in Punjab, India. In 2020 and 2021, a relatively large fraction of fire activity occurred during the MODIS/VIIRS overpass time window (13:00-14:30 LT; grey shading). In contrast, 2024 (in gold), and especially 2025 (in red), exhibit a pronounced shift toward increased late afternoon burning, with peak activity occurring around 16:30-17:00 LT. Panel (b) zooms in on the VIIRS overpass time window using a logarithmic scale, revealing a substantial decline in MSG-IODC FRP during 2024 and 2025, with some periods showing little to no detectable fire activity. Panels (c) and (d) present spatial maps of MSG-IODC FRP in Punjab for 2024 and 2025, respectively. These maps demonstrate that the marked increase in FRP observed in 2025 is not driven by a small number of anomalous pixels. Instead, the increase is spatially widespread and concentrated across the southern portion of Punjab, where most burning activity occurs.

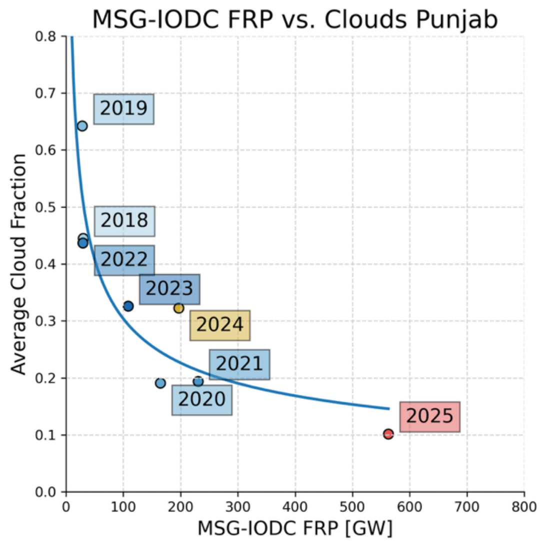

Figure 4. Seasonal total MSG-IODC FRP plotted against MAIAC MCD19A2 seasonal averaged cloud fraction over Punjab reveals a pronounced inverse power-law relationship. The exceptionally low cloud fraction during the 2025 fire season (~10%) may have contributed to the record-high FRP detected by MSG-IODC, suggesting that interannual variation in cloud cover has a major influence on the observed fire signal. To exclude the low-fire period at the end of the season and thus avoid meaningless FRP-cloud relationships, seasonal mean FRP and cloud fraction were calculated only over the period that covered 95% of the cumulative seasonal FRP.

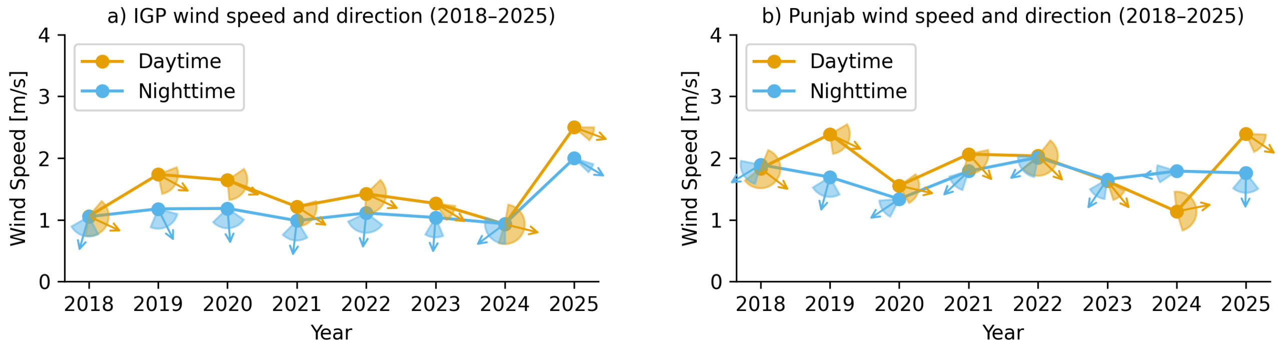

Figure 5. Mean WRF-Chem (nudged by NCEP FNL) 10-meter vector-averaged wind speed [m/s] and wind direction (direction towards) for the entire IGP (panel a) and Punjab (panel b). The average over the first 15 days of November is taken when fire activity is the highest. Wedges indicate the ±1σ directional standard deviation, providing a measure of day-to-day wind direction variability. Across the IGP, 2025 was characterized by persistently stronger eastward transport (up to 2.5x larger than previous years) during both daytime and nighttime, and little directional variability throughout the fire season. In contrast, 2024 exhibited the weakest net transport since 2018 and substantially greater directional variability, with predominantly eastward flow during the day and southwestward flow at night. A similar pattern was observed over Punjab, where 2024 was marked by opposite and highly variable wind directions. The contrasting meteorological conditions between 2024 and 2025 likely contributed to substantially enhanced ventilation and transport of cleaner air into Punjab and the broader IGP in 2025. This interpretation is supported by HYSPLIT trajectory simulations, accumulation sensitivity analyses and MERRA-2 meteorological reanalyses assessment presented in the SI.

Supporting Information Text

Satellite observations

Total column carbon monoxide (CO) Level 2 product is used from the TROPOspheric Monitoring Instrument (TROPOMI) aboard the Sentinel-5 Precursor. TROPOMI retrieves total column CO from measurements of reflected solar radiation in the shortwave infrared (SWIR) spectral range (2305-2385 nm) using the SICOR retrieval algorithm[31,51]. The product provides near-global daily coverage at 7 by 5.5 km resolution in nadir and is sensitive to CO throughout the troposphere, including the boundary layer under clear-sky conditions. Validation studies have shown good agreement between TROPOMI CO columns and independent ground-based observations from the NDACC and TCCON networks, with performance meeting mission accuracy requirements of <10ppb and correlation coefficient >0.9[66]. We retained only retrievals with recommended quality assurance values of 0.7 and larger, meaning good retrieval over low level clouds and clear-sky conditions.

For aerosol loading, we used aerosol optical depth (AOD) retrievals from the Visible Infrared Imaging Radiometer Suite (VIIRS) aboard the Suomi National Polar-orbiting Partnership (Suomi-NPP) satellite. VIIRS Deep Blue AOD at 550nm are derived from multispectral observations in the visible and shortwave-infrared wavelengths[33].

For LEO-based fire activity, we used Fire Radiative Power (FRP reported in megawatts) retrievals derived from the active fire products of the Moderate Resolution Imaging Spectroradiometer[28] (MODIS, Collection 6) aboard the Terra and Aqua satellites and VIIRS[29] onboard the Suomi-NPP, NOAA-20, and NOAA-21 satellites. MODIS detects thermal anomalies at approximately 1 km spatial resolution and provides per pixel FRP estimates based on mid-infrared radiance measurements. Only MODIS retrievals with confidence level over 50 were used. VIIRS active fire products complement this record using improved spatial resolution (375 m) and enhanced sensitivity to smaller and lower-intensity fires. Only nominal and high confidence VIIRS retrievals were used.

For burned area estimates, we used the MODIS Collection 6 MCD64A1 burned area product[44], VIIRS VNP64A1 product[46] and Sentinel-3 SYN version 1.1 gridded product[47]. The MCD64A1 product maps the spatial extent and approximate date of vegetation burning globally at 500 m spatial resolution. It combines daily surface reflectance observations from the Terra and Aqua MODIS instruments with active fire detections to identify persistent burn induced changes in surface reflectance and delineate burned areas. By integrating the detected surface reflectance with active fire information, the product provides monthly burned area. VNP64A1 derives monthly burned area from observations acquired by VIIRS aboard the Suomi-NPP satellite. The product identifies similarly burned area through the detection of temporal changes in surface reflectance and thermal characteristics at a spatial resolution of 500 m. Compared with MCD64A1, VNP64A1 benefits from the improved radiometric performance and active fire detection capabilities of VIIRS. The Sentinel-3 SYN maps the spatial extent of vegetation fires by combining observations from the Sentinel-3 Ocean and Land Colour Instrument (OLCI) and Sea and Land Surface Temperature Radiometer (SLSTR) sensors. The sensors operate at 300m spatial resolution but the used product of burned area is provided on a grid of 0.25° x 0.25°.

For geostationary-based fire activity, we used FRP retrievals from the Spinning Enhanced Visible and InfraRed Imager[34] (SEVIRI) onboard the Meteosat Second Generation (MSG) satellite operating in the Indian Ocean Data Coverage (IODC) configuration. Until 1 July 2022, coverage was provided by Meteosat-8 at 41.5°E and was extended by Meteosat-9 from 1 July 2022 onward at 45.5°E. The SEVIRI FRP product is generated using the Fire Thermal Anomaly (FTA) algorithm, which identifies active fire pixels from infrared observations. A key advantage of SEVIRI is its high temporal sampling at 15-min intervals, which enables characterization of the full diurnal cycle of fire activity and captures shortlived fire behavior that is often missed by LEO sensors. We used the FRP-PIXEL product for FRP estimates for individual fire detections. The spatial resolution around Punjab is >10 km, an order of magnitude coarser than MODIS and VIIRS.

The daily cloud fraction was derived using the gridded MODIS Multi-Angle Implementation of Atmospheric Correction[48] (MAIAC) MCD19A2 product at 0.05° x 0.05° grid. It provides a measure of the average cloud cover during Aqua and Terra overpass.

Surface observations

For surface air quality observations, we use measurements from the Aakash Project's[16,43] Compact and Useful PM2.5 Instrument with Gas sensors (CUPI-G) network deployed across Punjab, Haryana, and the Delhi NCR. The CUPI-G instruments provide continuous, high-frequency measurements of PM2.5 and CO concentrations and were specifically designed to characterize the spatial and temporal evolution of air pollution associated with crop residue burning and regional transport. During postmonsoon observation campaigns in the period 2022-2024, approximately 30-32 sensors were deployed across northwestern India, providing dense coverage of both source regions and downwind receptor areas. The network complements satellite observations by providing continuous in situ measurements under conditions where aerosol and fire retrievals may be obscured by cloud cover or limited by satellite overpass frequency. The PM2.5 measurements are based on an optical particle sensor calibrated for ambient conditions, while the accompanying gas sensors provide CO observations.

For surface visibility, we used observations from the meteorological station at Amritsar, Punjab (site identifier: INI0000VIAR), obtained from NOAA's National Climatic Data Center's Climate Data Online program (https://www.ncdc.noaa.gov/cdo-web/). Visibility is reported as the horizontal distance in km at which a prominent object can be seen and identified against the horizon sky. It provides an independent surface-based metric for evaluating the temporal evolution of aerosol pollution.

Meteorological analyses

To investigate the relationship between CO emissions, atmospheric CO columns observed by TROPOMI, and prevailing meteorological conditions, we use version 4.7.1 of the Weather Research and Forecasting model coupled with chemistry (WRF-Chem) as the forward modeling framework[52]. Simulations were performed for northern India during the postmonsoon season (September-December) for each year from 2018 through 2025 using a horizontal grid spacing of 30 x 30 km^2. Chemical transformations of CO and related species were represented using the Regional Acid Deposition Model, second generation for gas-phase chemistry[53] (RADM2). To maintain consistency between the simulated atmospheric state and the large-scale meteorological analyses, grid nudging toward the National Centers for Environmental Prediction (NCEP) Final (FNL) Operational Global Analysis dataset[54] was applied at hourly intervals throughout the simulations.

The model employs a terrain-following eta-coordinate vertical structure with enhanced resolution in the lower atmosphere to better represent boundary layer processes. A total of 33 vertical levels were used, with the model top located at 5000 Pa. Above this altitude, trace gas concentrations were assumed to remain constant and equal to those in the uppermost model layer.

Physical parameterizations included the Morrison two-moment microphysics scheme[55] and the Rapid Radiative Transfer Model for GCMs[56] (RRTMG) for both shortwave and longwave radiation. Surface-atmosphere exchanges were simulated using the Unified Noah Land Surface Model[57] (LSM) together with the revised MM5

Monin-Obukhov surface layer formulation[58]. Planetary boundary layer dynamics were represented using the Yonsei University (YSU) boundary layer scheme[59]. For consistency with satellite observations, modeled CO profiles were vertically regridded and convolved with the corresponding TROPOMI averaging kernels.

Initial and lateral boundary conditions for CO and other chemical species were obtained from the CAMS atmospheric composition reanalysis[60] and interpolated onto the WRF-Chem grid. Biomass burning emissions were prescribed using daily emissions from the GFED5 dataset[61], provided at 0.25° x 0.25° spatial resolution. For years up to and including 2022, emissions were derived from the standard GFED5 product, which incorporates updated burned area information, improved estimates of fuel loading, and revised emission factors. For the final years, emissions were obtained from the GFED5 near-real-time (NRT) product, which estimates burned area and associated emissions from VIIRS active fire observations using biome- and region-specific relationships calibrated to maintain consistency with the GFED5 historical record[62].

Anthropogenic emissions were taken from the CAMS-GLOB-ANT v5.1 inventory[63], available at 0.1° x 0.1° resolution, while biogenic emissions were obtained from CAMS-GLOB-BIO v3.0[64] at 0.25° x 0.25° resolution. All emission inventories were spatially regridded to the WRF-Chem domain and model resolution of 30 x 30 km^2 before being incorporated into the simulations.

HYSPLIT trajectory[65] analyses were used to assess regional transport and atmospheric residence times. Three air parcels were tracked moving back in time starting at the centers of Punjab, Haryana, and Uttar Pradesh. All trajectories covered the period 29 October 01:00 UTC - 8 November 01:00 UTC in 2024 and 2025. Images were generated on the HYSPLIT online computing platform maintained by the NOAA Air Resources Lab: https://www.ready.noaa.gov/HYSPLIT_traj.php.

Planetary boundary layer and wind diagnostics were obtained from the Modern-Era Retrospective Analysis for Research and Applications, Version 2 (MERRA-2) reanalysis[67]. We used hourly 10 m wind fields and planetary boundary layer height for October-November 2018-2025 over northern India. The ventilation coefficient, a proxy for atmospheric vertical dispersion, was calculated as the product of the planetary boundary layer height and the 10 m wind speed. All statistics were computed as local-time averages over the Punjab state polygon.

Accumulation sensitivity

To quantify the contribution of regional biomass burning to CO accumulation over the Punjab and IGP, two sets of WRF-Chem simulations were run for each year. In the baseline configuration, all emission sources and boundary conditions were included throughout the model domain. In the sensitivity configuration, fire emissions within the IGP states of Punjab, Haryana, Uttar Pradesh, Bihar, and West Bengal were removed, while all other emissions and boundary conditions remained unchanged. Comparison of these paired simulations enabled a direct assessment of the influence of biomass burning on CO concentrations across the IGP.

Accumulation sensitivity was derived by taking the CO concentration over Punjab from the baseline simulation and subtracting that by the no-fire simulation, and normalizing the resulting concentration by the magnitude of the Punjab fire emissions. Because this study demonstrates that an increasing fraction of crop residue burning occurs outside the VIIRS overpass window, the used GFED5-NRT emissions in WRF-Chem are likely to underestimate the absolute magnitude of agricultural fire emissions during these years. This limitation primarily affects the absolute simulated CO concentrations. However, because the accumulation sensitivity metric is normalized by the corresponding fire emissions, it is intended to isolate and quantify the efficiency of atmospheric accumulation under different meteorological conditions rather than evaluate the absolute emission magnitude.

Fire emission inventories

Regional postmonsoon fire emission estimates for Punjab were compared using three inventories: GFAS[20], GFED4s[21], and the already mentioned GFED5[61] (and GFED5-NRT for 2023-2025). GFAS derives emissions from MODIS FRP, which is converted to dry matter burned and emissions using biome-specific conversion factors and emission factors. GFED4s estimates emissions from MODIS burned area, supplemented with a statistical small fire correction based on active fire detections and CASA-derived fuel loads. After 2016, emissions are estimated from empirical relationships with MODIS active fire observations (beta product) and climatological fire emissions.

Supporting Information Figures

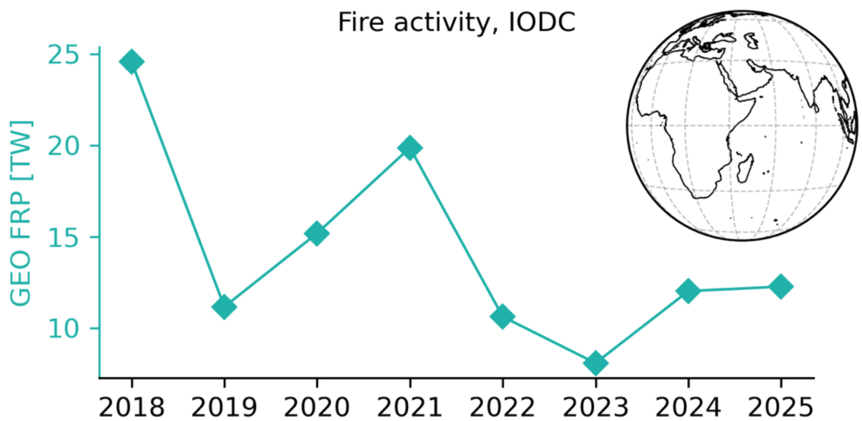

Fig. S1. Eight-year time series of geostationary MSG-IODC FRP [TW] for the full Indian Ocean Data Coverage region (inserted projection) during November. The results show that the total IODC FRP in 2025 is moderate and comparable to that of 2024, suggesting the spike in fire activity in Punjab in 2025 (Figs. 2 and 3) is unlikely the result of a processing artifact or systematic error affecting the broader dataset.

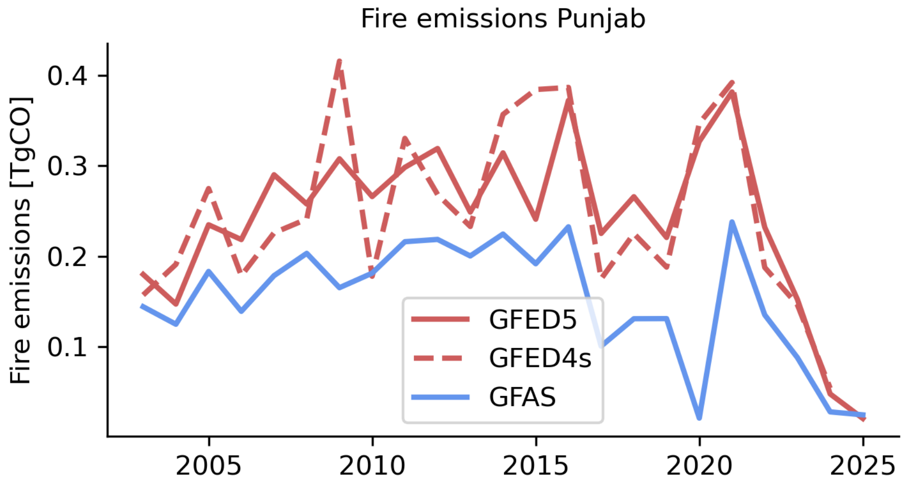

Fig. S2. Comparison of regional fire emission estimates during the postmonsoon fire season from GFED5+GFED5NRT (solid red), GFED4s (dashed red) and GFAS (solid blue) for Punjab. All inventories report a large drop in emissions from 2022 onward, reflecting the limitations of LEO satellite observations in capturing the increasingly late afternoon burning activity. The GFAS 2020 drop is somewhat anomalous and its cause is unclear, since the detected MODIS and VIIRS fire activity was high (see Fig. 2a).

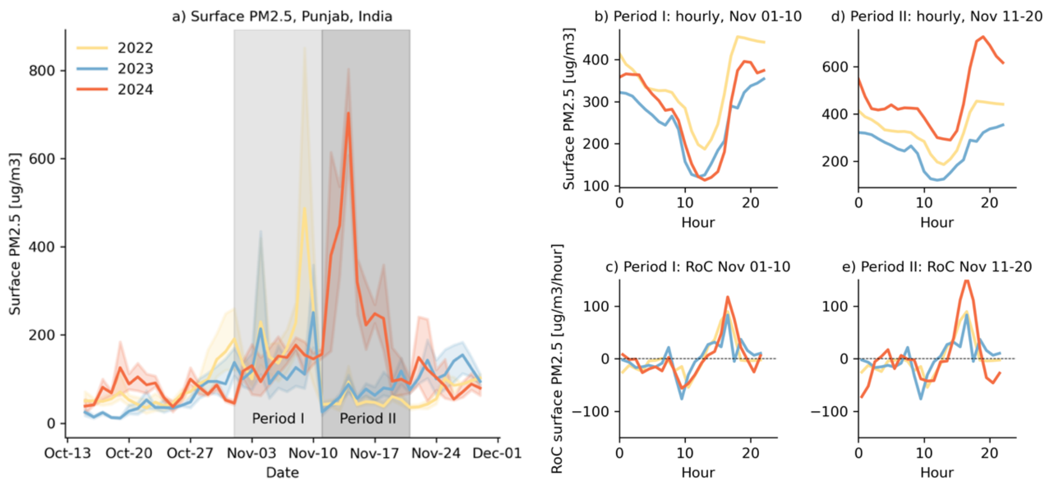

Fig. S3. Panel (a) shows daytime-averaged PM2.5 concentrations highlighting two distinct 10-day periods: Period I (1-10 November) with elevated PM2.5 in 2022 and 2023, and Period II (11-20 November) where 2024 exhibits markedly higher PM2.5 levels, corroborating the intense pollution episode seen from space (Fig. 1a-b). Panels (b) and (d) display the average diurnal PM2.5 cycles for Periods I and II, respectively, while panels (c) and (e) show the corresponding rates of change (RoC). A sharp late afternoon increase in PM2.5 (16:00-17:00 LT) aligns with MSG-IODC fire activity peaks (Fig. 3), especially pronounced in 2024, with Period II's rate of change nearly double that of earlier years. No data were available for 2025.

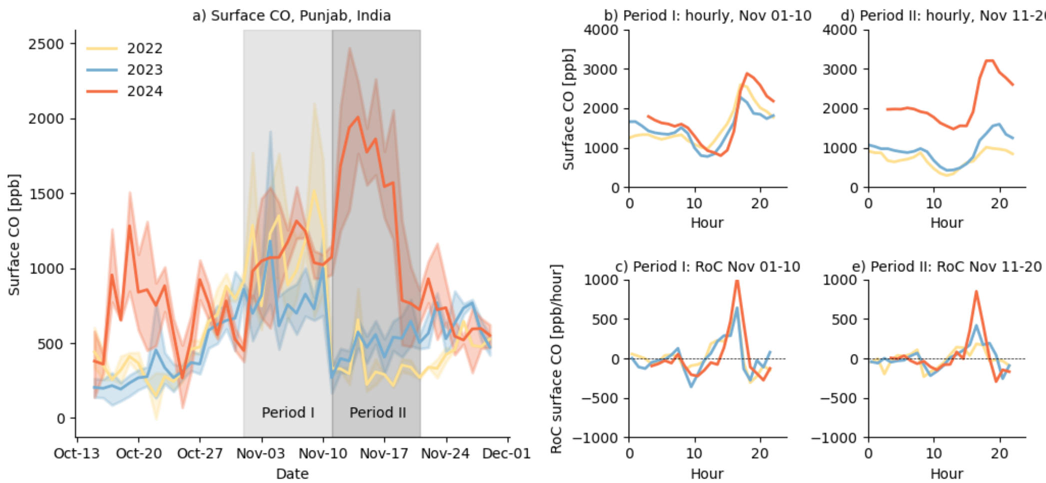

Fig. S4. Similar to Fig. S3, but now for ground-based CO measurements.

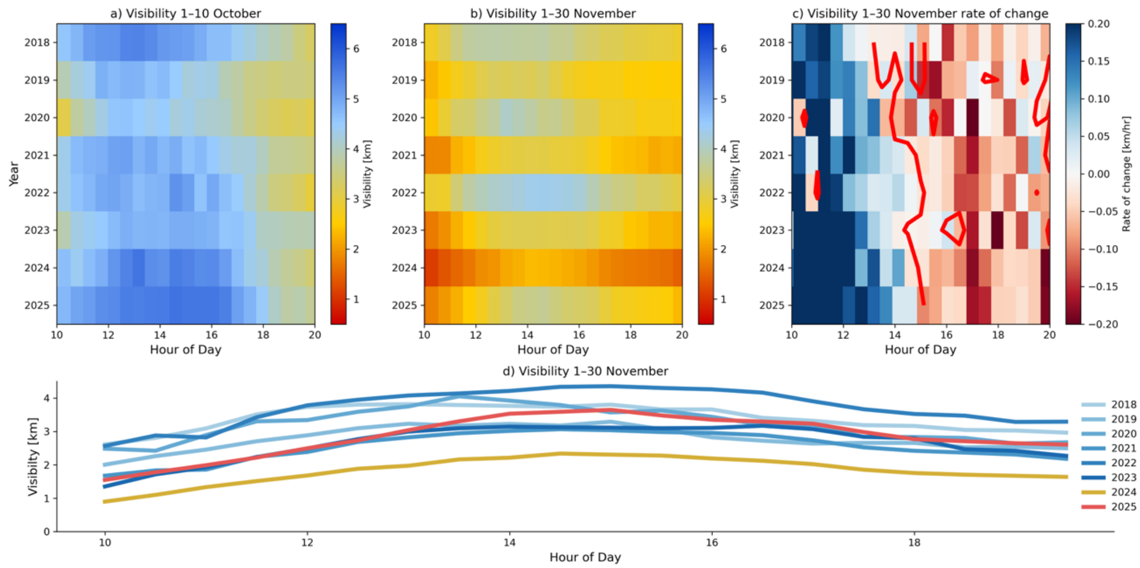

Fig. S5. Daytime visibility measurements at 30-minute intervals from the Amritsar monitoring station (INI0000VIAR) in Punjab before the fire season (1-10 Oct panel a), during the fire season (1-30 Nov; panel b), and the corresponding hourly rate of change in visibility during the fire season (panel c). Contours of inflection point (rate of change = 0) are shown by the red curves. Panel (d) presents the averaged daytime visibility time series for each year during the fire season (1-30 Nov). Although visibility at this one site does not provide a one-to-one correspondence with the satellite-derived pollution metrics shown in Fig. 1, it broadly reflects the observed interannual variability in air quality. Most notably, visibility during the 2024 fire season (gold curve) was exceptionally poor, consistent with the record-high CO and AOD levels observed from satellite measurements in Fig. 1. In contrast, visibility in 2025 (red curve) was quite average for this time of year, in agreement with the meteorological conditions discussed later in the SI, which likely enhanced atmospheric ventilation and pollutant dispersion.

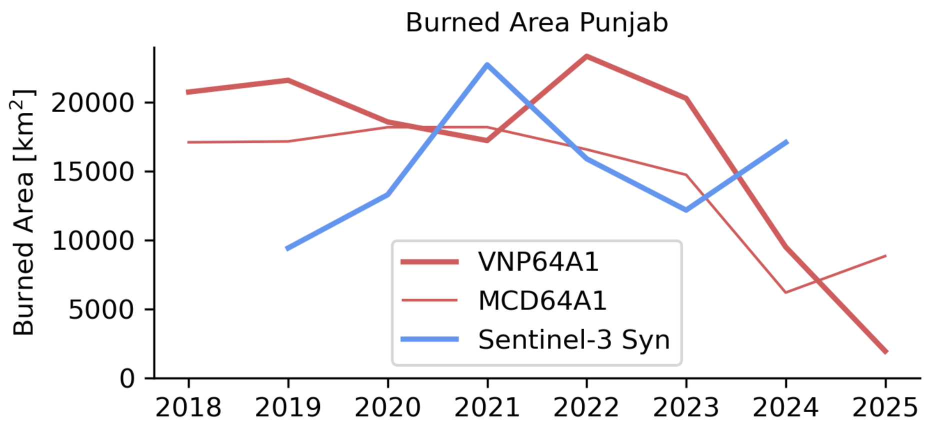

Fig. S6. VIIRS VNP64A1 (bold red), MODIS MCD64A1 (red) and Sentinel-3 SYN (blue) burned area for Punjab, recorded for October and November between 2018-2025. S3 SYN only covers the period 2019-2024.

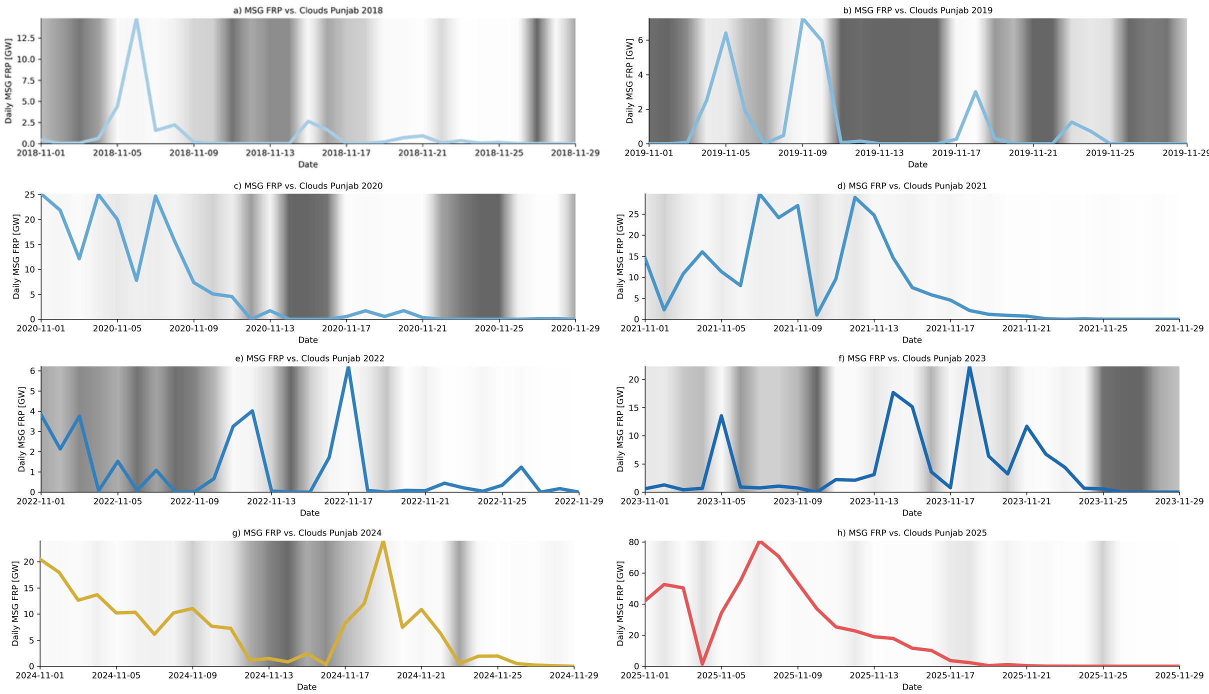

Fig. S7. Colored lines in panels (a-h) show time series of MSG-IODC FRP during November in the fire season (2018-2025) in Punjab. The background shading indicates the mean MAIAC MCD19A2 daily cloud fraction, with darker shades representing greater cloud cover. Across all years, FRP peaks are generally associated with periods of relative clear-sky conditions. The 2025 season is particularly notable, exhibiting persistently high FRP during the first half of November when cloud fractions were low. This temporal correspondence between enhanced observed fire activity and reduced cloud cover helps explain the inverse power-law relationship between cloud fraction and FRP reported in Fig. 4 of the main text.

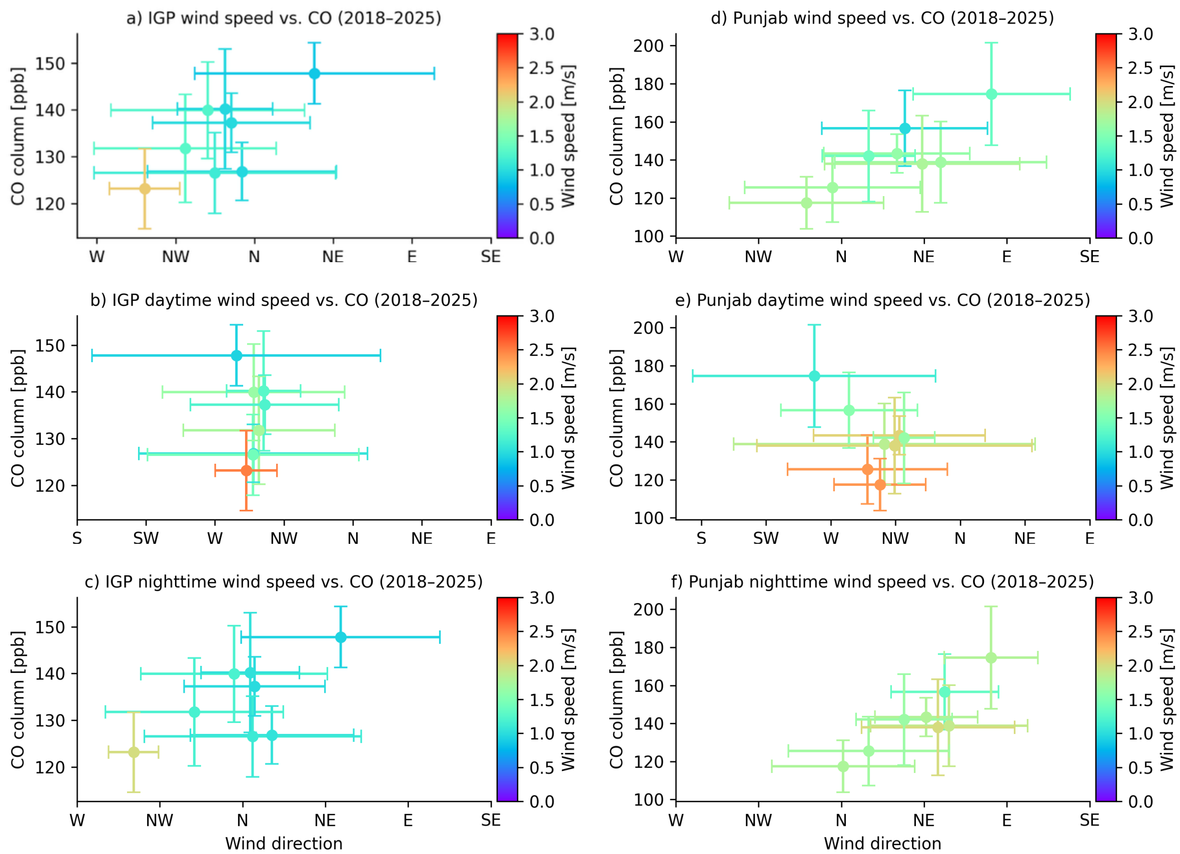

Fig. S8. Panels (a-c) show mean TROPOMI CO column concentrations over the IGP during the fire season as a function of wind direction (x-axis; direction the wind is coming from) and wind speed (color scale; m/s). Wind speed and direction were derived from hourly WRF-Chem simulations nudged with NCEP FNL reanalysis data. Panel (a) uses wind data from the full diurnal cycle, panel (b) from daytime hours only, and panel (c) from nighttime hours only. Panels (d-f) show the corresponding analysis for Punjab alone. Note the horizontal axis for the middle panels is shifted compared to the upper and lower panels. For the IGP, lower CO concentrations are generally associated with strong eastward (westerly) winds when wind directions exhibit relatively little day-to-day variability. Daytime CO levels appear to be more strongly influenced by wind speed than by wind direction. Over Punjab, the lowest CO concentrations are typically associated with southward (northerly) directed winds, suggesting more efficient ventilation under these conditions.

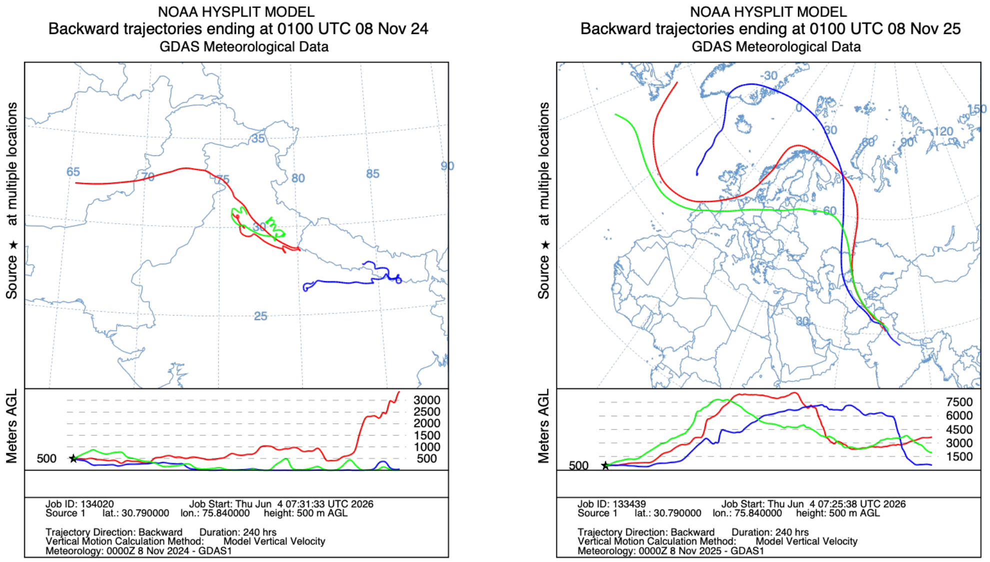

Fig. S9. HYSPLIT particle backward trajectories integrated for 10 days, coverging the period between 29 October - 8 November in 2024 (panel a) and 2025 (panel b). The colored trajectories start near the centers of three major IGP states: Punjab (red), Haryana (green), and Uttar Pradesh (blue). In 2024, the trajectories indicate weak and variable transport pathways at low vertical levels, with air parcels remaining over the IGP for most of the 10-day simulation period. This results in long residence times and limited ventilation. In contrast, the 2025 trajectories start far upstream over the Atlantic Ocean and are transported rapidly toward the IGP by persistent eastward flow. The air parcels stay over the IGP states for a very brief time, indicating substantially enhanced ventilation and a greater influx of relatively clean background air into the region. These results are consistent with the WRF-Chem wind analysis presented in Fig. 5 and provide independent evidence for markedly stronger atmospheric ventilation during the 2025 fire season. Meteorological data came from NCEP GDAS model. These images were generated on the HYSPLIT online computing platform maintained by the NOAA Air Resources Lab: https://www.ready.noaa.gov/HYSPLIT_traj.php.

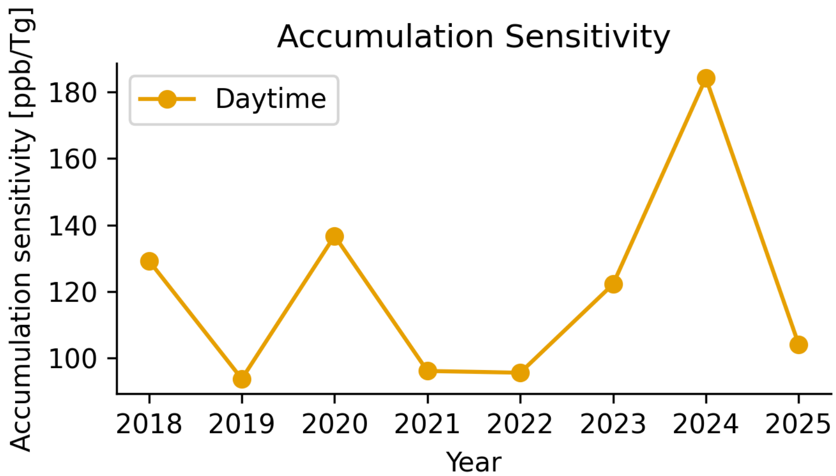

Fig. S10. Accumulation sensitivity [ppb/Tg CO] over Punjab during the first 15 days of November, defined as the change in atmospheric CO column concentration per unit of fire CO emissions from GFED5. High sensitivity values indicate that a given amount of fire emissions produces a larger increase in atmospheric CO concentrations, reflecting weaker ventilation and pollutant dispersion. Conversely, low sensitivity values indicate more efficient ventilation, resulting in smaller concentration increases for the same emission amount. Note that in contrast to 2024, 2025 was characterized by much more air ventilation, explaining the much lower CO and AOD levels observed in Fig. 1. Accumulation sensitivity was quantified using two WRF-Chem simulations: (1) baseline scenario that included all anthropogenic, biogenic, and fire emissions everywhere; and (2) a sensitivity scenario with anthropogenic and biogenic emissions included both inside and outside the IGP, together with only fire emissions outside the IGP, but those within the IGP removed. The sensitivity metric was calculated as the difference in simulated CO concentrations over Punjab between the two scenarios divided by the corresponding Punjab CO fire emissions, thereby isolating the atmospheric response to regional fire activity.

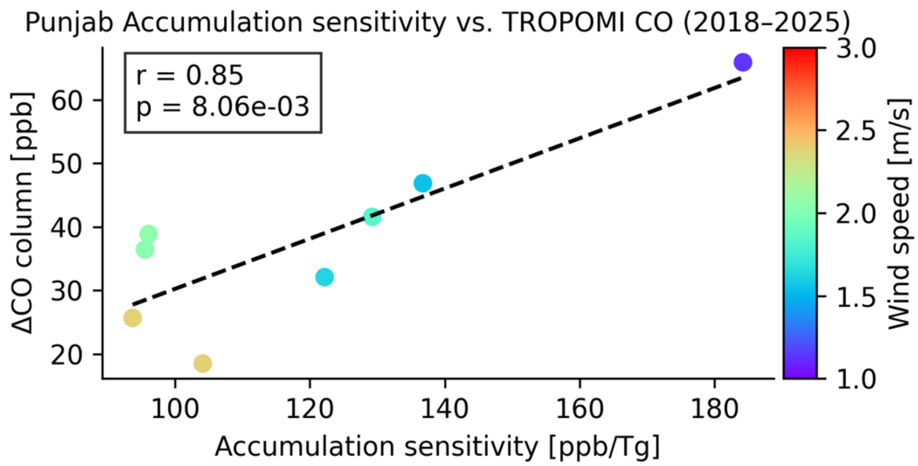

Fig. S11. Seasonal accumulation sensitivity [ppb/Tg CO] derived from Fig. S10 versus TROPOMI CO column enhancements in November [ppb], calculated relative to pre-season CO levels averaged over 1-10 October in Punjab. Colored markers denote vector-averaged 10 m wind speed [m/s] from WRF-Chem simulations nudged with NCEP FNL reanalysis data. In general, with a Pearson correlation of r=0.85 and p=0.008, lower CO enhancements are observed under conditions of reduced accumulation sensitivity and stronger winds, consistent with enhanced atmospheric ventilation and pollutant dispersion (e.g., in 2019 and 2025).

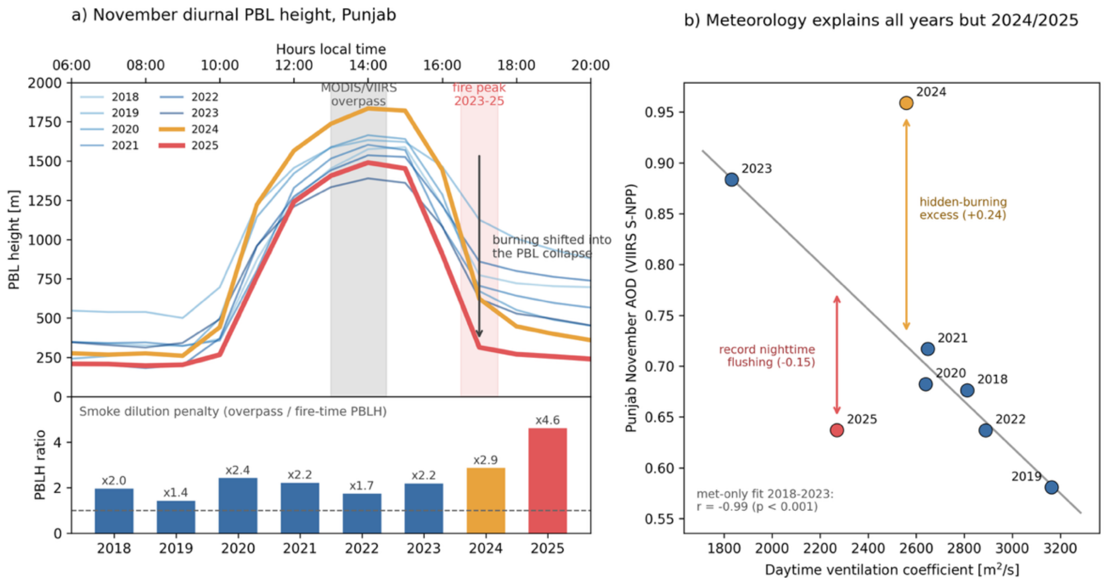

Fig. S12. Planetary boundary layer (PBL) and ventilation context for the shift in burn timing, derived from MERRA-2 reanalysis (Punjab state means, November, local time). Panel (a): mean diurnal cycle of PBL height for each year, with 2024 (orange) and 2025 (red) highlighted. Shaded bands mark the MODIS/VIIRS overpass window (13:00-14:30 LT, gray) and the late afternoon fire peak observed by MSG-IODC in 2023-2025 (16:30-17:30 LT, red). The lower panel shows the smoke dilution penalty, i.e., the ratio of November-mean PBL height in the VIIRS overpass window to that at the fire peak later afternoon (dashed line indicates equal depth). The shift in burning coincides with the afternoon collapse of the PBL. Smoke released in the late afternoon is mixed into a PBL typically two or more times shallower than at the early afternoon overpass time, and in 2025 — the year with the earliest and deepest collapse of the record — this factor reached 4.6, corresponding to a late-afternoon PBL of only ≈300 m. Panel (b): Punjab November AOD (VIIRS S-NPP) versus the daytime ventilation coefficient (PBL height x 10 m wind speed). For 2018-2023, ventilation alone explains nearly all interannual variability in AOD (gray line; $r = -0.99$, $p < 0.001$). The two anomalous years deviate in opposite directions: 2024 AOD lies +0.24 above the meteorology-only expectation, consistent with unusually stagnant conditions in combination with substantial fire emissions undetected by LEO sensors, whereas 2025 AOD lies −0.15 below it, consistent with unusually persistent nighttime eastward transport ventilating the IGP. Notably, 2025 combined a shallow and stable boundary layer (panel a), conditions that would normally favor accumulation, with the most persistent nighttime eastward transport of the record (Fig. 5 and SI Fig. S9). Its position below the meteorology-only relationship in panel (b) therefore isolates horizontal advection, rather than vertical mixing, as the process controlling the low pollution levels in 2025.

SI References

All references are listed in the main text.